1. Introduction

After numerical studies showed that global climate change is sensitive to small changes in sea surface temperature (T_s), considerable effort has been devoted to examine the role of surface fluxes in changing upper ocean heat balance and T_s, particularly in the tropical Pacific where interannual signals, such as El Niño Southern Oscillation (ENSO), have major economic and ecological impacts [e.g., Niiler and Stevenson, 1982; Leetma, 1983; Weare, 1983; Meyers et al., 1986; Godfrey and Lindstrom, 1989]. Studies in the past were hampered by a lack of basin-wide observations. In an attempt to overcome this undersampling problem, Liu [1988] and Liu and Gautier [1990] computed the two major components of surface thermal forcing, namely latent heat (E) carried by evaporation, and net solar irradiance from the sun (S), using satellite data. Their studies were confined to the central and eastern tropical Pacific, because the microwave radiometer data available at that time had geographically dependent errors and the geostationary Satellite GOES-W had only limited coverage. The interest in the relation between surface heat fluxes and Ts, however, is not confined to the tropical ocean [e.g., Cayan, 1992]. Recent availability of satellite data from the International Satellite Cloud Climatology Project (ISCCP) and from the Special Sensor Microwave Imager (SSMI) on the operational spacecraft of the Defense Meteorological Space Program make it possible to derive E and S with adequate duration to study annual and interannual changes over global oceans.

Over global oceans T_s rarely rises above 30°C, and a large area in the western Pacific and the east Indian Oceans, hereafter referred to as the warm pool, has relatively uniform T_s between 28° and 30°C. Recently, Ramanathan and Collins [1991], hereafter referred as RC, found spatial correlation between local cloud forcing and T_s across the entire tropical Pacific and postulated that cirrus clouds are the main mechanisms in keeping local T_s at an equilibrium value, and also in saving the Earth from run-away

greenhouse warming. Their "thermostat hypothesis" led off renewed debates. Trenberth [1992] argued that the feedback mechanism is not local; the ascending and descending branches of large-scale atmospheric circulation have opposing effects on cloud. Wallace [1992] suggested that the efficiency of large-scale circulation in redistributing the energy makes it unnecessary to have the cirrus cloud as a thermostat; uniform ocean temperature is just a reflection of uniform atmospheric temperature. Fu et al. [1992] also challenged the results of RC and, using observations from ISCCP, demonstrated that there is no cloud feedback when averaged over the tropical Pacific; cloud forcing was controlled more by changes in large-scale atmospheric circulation than directly by local T_s. Waliser and Graham [1993] underscored the role of convection and they inferred, using satellite observations of outgoing longwave radiation and highly reflective cloud, that the highest sea surface temperatures are associated with reduced convection and cloud. The four studies, Trenberth [1992], Wallace [1992], Fu et al. [1992], and Waliser and Graham [1993] emphasized the importance of evaporation in regulating Ts, a process which was not considered important by RC.

Evaporation from the ocean has long been suggested as the mechanism responsible for the high cutoff in the frequency distribution of global T_s. The most common explanation is based on the non-linear relation between temperature and saturation humidity, the Classius-Clapeyron (CC) function [Fleagle and Businger, 1963]. The capacity of the atmosphere in holding water vapor increases much more rapidly at high temperatures than at low ones. The inference is that evaporation will increase sharply with temperature over warm waters. The latent heat carried by evaporation cools the ocean and provides a negative feedback [Priestley, 1966]. In idealized conceptual studies [Newell, 1979], an equilibrium threshold T_s was derived by holding atmospheric wind speed, temperature, humidity, and irradiance constant and letting E rise rapidly with T_s. The efficiency in removing accumulated moisture in the atmosphere was not

considered. The significance of negative feedback of E on Ts has not been vigorously tested because of the lack of field observations.

In past studies on negative feedback, cloud forcing and convection were inferred from satellite observations of the top-of-atmosphere properties. The influences of convective ventilation and cloud cover on T_s must be manifested through surface fluxes of latent heat and radiation. Our main objective is to examine the relation between the two major surface heat flux components and Ts, making use of the SSMI and ISCCP data, The relations also provide an opportunity to check on the various postulations and analyses in the "thermostat debate", which are entirely based on annual and interannual variations.

2. **Temporal Correlation to be Tested**

There are two common postulations related to the natural thermostat. Firstly, Ts has to be able to change the fluxes significantly, either through turbulence or convection, regardless of other conditions, Simply, any increase in Ts has to result in a decrease in S through an increase in cloud; that means a negative correlation between Ts and S, An increase in T_s should increase evaporation, which means a positive correlation between evaporation and Ts. On a monthly time scale, convection and turbulent transfer is fast and the correlation should be contemporary. The relation between E and Ts is known and, for all practical applications, can be represented by the bulk formula:

$$E = \rho_a C_E L u \Delta q \qquad (1a)$$

$$Aq = q_s - q_a = [Q(T_s) - rQ(T_s+\Delta T] \qquad (1b)$$

where C_E is the transfer coefficient, r is the relative humidity, ρ_a is the air density, L is the latent heat of vaporization, u is the wind speed, q is the specific humidity, T is the potential temperature, ΔT and Aq are the sea-air temperature and humidity differences, Q(T) represents the saturation specific-humidity as a function of temperature T, subscript 's' represents the value at the sea-air interface, and subscript 'a' represents the value at a reference level in the atmospheric constant flux layer (approximately 50 m thick). E would increase with T_s at a rate governed by the CC function, only if u, AT, and r are relatively constant. If the u and q_a effects are stronger, there will be positive correlation between u and E, and negative correlation between q_a and E. All these correlations will be examined later.

Secondly, the fluxes should have significant impact on changing T_s through upper ocean heat balance. The importance of various terms in the upper ocean heat balance at various locations and seasons has been extensively studied through observation and modeling. A simplified representation of the heat balance in a well-mixed layer of the upper ocean of depth h with temperature approximately equal to T_s is

$$\rho_w ch \frac{dT_s}{dt} = S - E + A + B \qquad (2)$$

where t is the time, p_w is the water density, and c is the isobaric specific heat of water. A represents heat transported (by advection, turbulence, or diffusion) into this layer, both horizontal and vertical. The sum of sensible heat flux and longwave radiation at the surface and the radiation penetration through the bottom" of the mixed layer are represented by B. If E is dominant relative to other terms on the right side of Eq. 2, and if h is relatively constant, there should be a significant negative correlation between E and temperature tendency dT_s/dt. On the other hand, if S is more important, there should be a positive correlation between S and dT_s/dt. Over most of the ocean, the annual cycle of T_s

is sinusoidal and dT_s/dt is 90° off phase. That means we could replace the tendency with lag T_S and get the same correlation. It takes time to warm up the mixed layer.

We should be able to shed some lights on the causes and effects of Ts changes by examining simultaneous and lag correlations. The temporal relation between T_S and fluxes in seasonal cycles and in ENSO anomalies will be examined in Sections 6 and 7.

3. **Data and Flux Computation**

The basic method of computing E from satellite data was described and validated in Liu [1988]. According to Eq. 1, the estimation of E requires the knowledge of C_E and the measurements of u, q_a, and Ts. In this study, C_E is determined by a surface layer turbulent transfer model which accounts for the transition from rough flow (moderate and high winds) to smooth flow (low winds) and the moisture-induced atmospheric density stratification [Liu et al., 1979]. In this model, C_E is roughly equal to 1.3x10-3 [cf Friehe and Schmitt, 1976], increases sharply with decreasing wind when u<2 m/s, and decreases slightly at high winds. Recently, the high wind characteristic of the model was supported by measurements in the North Sea [Katsaros and DeCosmo, 1992] and the low wind characteristic was found to be in excellent agreement with field measurements in" the Bismarck Sea [Bradley et al., 1991]. The transfer coefficient depends on atmospheric density stratification, which is affected by air temperature. Air temperature used in the computation E was derived from q_a with **the** assumption of r=80%. The error in E introduced by this assumption is relatively small since air temperature has only a secondary effect, through stability of the atmosphere. The validity of using monthly parameters instead of instantaneous measurements in this model was tested in subtropical and temperate oceans using time series from weather ships [Esbensen and Reynolds, 198 1]. The errors due to the neglected high frequency variance are found to be small.

This is in agreement with studies using continuous *in situ* measurements at two locations in the equatorial Pacific, one in the cold tongue in the east and the other at Truk Island in the convective region of the warm pool [Liu, 1988]. Large variances have been observed during short-period, small-scale, and intermittent convections in the warm pool [e.g., Young et al., 1992], but there has not been any quantitative evaluation of the impact of these high frequency and small-scale variances on large-scale and monthly means to support or dispute the results of Liu [1988] and Esbensen and Reynolds [1981], because there is no long duration measurement of high temporal resolution.

Spaceborne sensors can measure u and T_s, but not q_a. A spaceborne microwave radiometer can measure the column integrated water vapor (W) accurately, The method to estimate E from satellite data is anchored on the feasibility of estimating q_a from W, The main rationale of relating q_a to W is the decoupling of the dominant mode of variability in humidity profiles, which is coherent through the entire atmospheric column from other modes, which are coherent only through limited depths [Liu et al., 1991], For periods longer" than two weeks, W is a good estimator of the humidity profiles and q_a. Other factors governing q_a variability, such as boundary layer changes, are important largely for shorter periods. A global relation between monthly q_a and W was derived using 17 years of radiosonde reports from 46 ocean meteorological stations [Liu, 1986]. The empirical relation was tested, using soundings from field experiments, routine ship reports, and atmospheric general circulation models [Liu, 1988; Hsu and Blanchard, 1989; Liu et al., 1992]; it was found sufficiently accurate to describe the annual and interannual variabilities. However, systematic errors were found in the western North Pacific and North Atlantic, and off the coast of Baja California during three summer months, resulting in overestimation of q_a [Liu, 1986; Liu et al., 1992]. The resultant stable stratification causes spurious suppression of turbulent transport and failure of the Liu et al. [1979] model. There are continuous efforts to evaluate this relation but the

work is handicapped by a lack of accurate humidity measurements over extensive areas of the ocean. For example, humidity climatologies are found to smear out the sharp gradients on the eastern tropical and subtropical southern oceans where *in situ* measurements have been extremely sparse [Liu et al., 1992].

The data set for this study consists of u and W from SSMI which were averaged into monthly fields with 1° latitude by 1° longitude resolution. The Ts data used are based on AVHRR (Advanced Very High Resolution Radiometers) observations, blended with available *in situ* measurements [Reynolds, 1988]. The Ts fields were spatially interpolated to SSMI grid positions using a Lagrangian interpolator [Press, et al., 1989] before computing E. This data set provides coverage over the global ocean for 47 months from July 1987 to June 1991, with December 1987 data missing. The period includes part of the warm phase and the entire cold phase of an ENSO episode. The Multichannel Sea Surface Temperature (MCSST) data products from AVHRR [McClain et al., 1985] were also tested. This data set has higher temporal and spatial resolutions than the blended data, but was found to include large deviations (from surrounding values) at high latitudes and therefore was not used in this study,

Cloud is the most serious uncertainty in the derivation of S. The techniques of retrieving S make use of the high sampling rate and high resolution of visible and infrared sensors on geostationary satellites. Global coverage requires data from five geostationary satellites run by 4 national agencies, with uncalibrated data in various formats. The task was forbidding until ISCCP set up the protocol for international data exchanges and provided calibrated standard products for the users [Rossow and Schiffer, 1991]. The method for computing S was described by Bishop and Rossow [1991]. Parameters from the renormalized ISCCP Cl data set, including solar zenith angle, atmospheric water vapor profile, ozone column abundance, cloud fraction, cloud optical thickness, visible

surface reflectance, surface type, and surface pressure, were usedto derive both clear and cloudy components of the radiance, at 2.5° latitude by 2.5° longitude and three-hour resolution, using a set of simplified radiative transfer equations. A daily sampling correction factor was applied to the sum of the two components to form daily values. Six percent of the downwelling solar flux was assumed to be reflected back. Monthly means from July 1983 to June 1990 interpolated to SSMI grid locations were used in this study.

4. **Ensemble Relation**

ScatterPlots of the ensemble of data have been commonly used to demonstrate the hypothesis on local feedback [e.g., RC; Waliser et al., 1993]. The ensemble of data in the form of average S and E as functions of T_s is shown in Figs. 1a and lb. The figures are produced by averaging all the values of S and E within each T_s bin of 0.5°C for 84 and 47 months, respectively. Data with T_s<0°C, from areas poleward of 60° latitudes, and from enclosed seas (e.g., Persian Gulf and Red Sea) are excluded, In the figures, the standard deviations are shown as error bars and the numbers of data in the bins are also plotted on logarithmic scales. At low Ts the fluxes are positively correlated with Ts. After E peaks at 25°C and S at 26°C, both fluxes decrease with increasing T_s. Above 29°C, S clearly increases with T_s, again. The two transitions in gradients roughly coincide with those of convective activities, derived from satellite observations of outgoing longwave radiation as a function of Ts by Waliser et al. [1993]. Their study shows that the correlation between convective activities and Ts is positive when 26.5 °C<T_s<29.5°C, but negative when T_s>29.5°C.

The positive gradients at lower temperatures (T_s < 26°C) in Fig. 1 may reflect the general tendency for evaporative cooling and solar heating to increase towards low latitudes. When 26°C<T_s<29°C, the warm ocean provides adequate moist static energy for the ascent of saturated air parcels from the surface ‘into deep convection [e.g., Betts

and Ridgeway, 1989]. The increase of convection within this range of warm temperature has been observed by Gadgil et al. [1984], Graham and Barnett [1987] and others. The increase in cloud cover associated with deep convection reduces solar heating. Similar negative correlation forms the basis of the hypothesis of RC. In this range of Ts, E does not increase with Ts according to the CC formula. The decrease of E with increase in Ts is in agreement with monthly mean and ENSO anomalies observed by Liu [1988] and the climatological distribution of E and T_s. Liu [1988] suggested that the high q_a and low u (convergence) in the center of organized convection or under the ascending branches of the Hadley and Walker circulation cause lower evaporation. At high temperature (T_s>29°C), S increases with increasing Ts, contrary to the local feedback postulation of RC. Waliser et al. [1993] examined the high Ts carefully and concluded that in the case of subsidence over warm ocean, suppression of cloud formation allows for the increase in S and Ts. E also increases slightly with Ts at the high temperatures. The exception is the last point (Ts>31°C,) which is derived from drastically less data, and it may be in error. Dry and subsiding air may be the reason for the slight increase of E with Ts, even over warm water. Fig. 1 shows that both E and S are positively correlated with Ts at low temperature, but the correlations turn negative at high temperature. However, this behavior is not universal and it breaks down as we separate the geographical from temporal variations.

5. Geographical Variability

Ensemble scatterplots like Fig. 1 do not distinguish the relation in temporal and spatial variabilities, nor do they reveal any remote relationship linked by circulation, To compare geographical variability, the distributions of monthly S, Ts and E for a typical boreal summer month (July 1989) and for a typical boreal winter month (January 1990) are compared in Fig. 2. The missing data in the North Pacific and North Atlantic shown

in the July E map (lower left) are the consequences of the q_a-W model failure discussed in Section 3. It is obvious from the figures that high T_s do not always correspond to high E and low S, as would be expected from the hypotheses of negative feedback. In a zonal belt just north of the equator marking the approximate position of the Intertropical Convergence Zone (ITCZ), in a region running southeast from Indonesia corresponding to the South Pacific Convergence Zone (SPCZ), and over the warm pool, E is relatively low where the highest T_s are found. High E is located in the Trade Wind regions of the winter hemisphere, but T_s in not the highest. The high evaporation south of Japan during winter months may reflect the dry continental air, as much as the warm water of Kuroshio. Positive relation is only found in the eastern tropical ocean basin where the cold water from upwelling reduces evaporation. The distribution is consistent with climatology derived from ship reports [e.g. Weare et al., 1981; Hsiung, 1986], with low E in the ascending branch of the Hadley and Walker circulations and high E in the descending branch and Trade Wind regions. The low values of E found in areas of high T_s were noticed by a few investigators [e.g., Cornejo-Garrido and Stone, 1977; Liu, 1990; Ramanathan and Collins, 1993]. The solar flux shows much stronger seasonal migration than T_s. Besides the major meridional variation, which is governed by seasonal change of solar incident angle, high S is found in regions of subsidence and clear sky and low S is found in ascendance and convection; such relation to atmospheric circulation is not obvious in T_s distribution.

The distributions of anomalies in two typical months during the warm and cold phases of ENSO are shown in Fig. 3, The anomalies are formed by removing the 'climatological' annual cycle from the monthly means. The 'climatological' annual cycles of various parameters are formed by averaging the parameters of each calendar month for the entire period in which data are available. Limited by data availability, the 'climatologies' of E and S are formed from different lengths (4 and 7 years respectively)

of data which do not completely overlap. Rather than using different T_s 'climatologies' for comparison with E and S, a single T_s 'climatology' derived from 9 years (January 1982-December 1992) of data was used, and the T_s anomalies discussed, hereafter, are based on this 'common climatology'. As shown in Fig. 3a and 3b, significant positive and negative S anomalies are found in the central equatorial Pacific, roughly where warm and cold Ts anomalies are also found (Fig. 3c and 3d), although the peaks of S anomalies are displaced to west of peaks T_s. However, in the eastern equatorial Pacific, where equally large T_s anomalies are found, no large S anomalies are observed, The displacements of S anomalies from T_s anomalies, which have been observed from outgoing longwave radiation, are likely to result from atmospheric dynamic response to surface heating, and the local feedback postulation is not sufficient to explain the relation between cloud and T_s. As with the monthly means, negative E anomalies in the central equatorial Pacific (Fig. 3e and 3f) are associated with positive T_s anomalies and vice versa, contrary to the negative feedback hypotheses. The centers of E anomalies are also displaced slightly to the west of the center of T_s anomalies. In the eastern equatorial Pacific, E anomalies are weak in July 1987 despite large T_s anomalies. However, negative anomalies are found over significant negative Ts anomalies in September 1988.

No simple universal relation between the, geographical distribution of surface fluxes and Ts, either for the monthly means or for the anomalies, is evident. It is interesting to note that while the ranges of monthly means are similar for E and S, the range of E anomalies is much larger than the range of S anomalies, as noticed by Fu et al. [1992].

6. **Seasonal Cycle**

To examine the relation of temporal variabilities between the fluxes and T_s, the distribution of correlation coefficients is used. While the correlation coefficient is simple to understand, it may not fully represent the non-linear relationship between two variables. As a test, the explained variances of high order polynomial regressions were selectively examined, but their patterns were largely similar to those of linear correlation coefficient and are not shown, Away from the equator, the monthly variation is dominated by the seasonal cycle. The monthly correlations between S and T_s and between S and dT_s/dt, shown in Fig. 4a and 4b, clearly reveal the cause and effect of seasonal Ts changes, For 84 pairs of independent data, a correlation higher than 0.28 would be significant at a 99% level. In reality, not all the data are independent and the correlation coefficient has to be higher than 0.28 to be significant. " Fig. 4a shows that, except in the near-equatorial oceans where interannual changes are important, there is no significant negative correlation between S and T_s. As we would expect, Ts does not drive the seasonal change of S, which depends largely on solar incident angle. However, the correlations between S and dTs/dt are significantly positive everywhere except in a narrow strip along the equator across all of the three oceans (Fig. 4b). The distribution is almost identical when dT_s/dt is replaced by T_s with a three-month lag.

The seasonal change of Ts is largely driven. by S, away from the equator. The annual cycles of S and T_s are clearly seen at 30°N,1 30°E and 40°S, 120°W, shown in Fig. 5a and 5c, with S reaching high value during summer and low value during winter. S leads T_s by a few months and, therefore, is in phase with dT_s/dt. This is the reason for the high positive correlations. At the equator and 0° longitude, in the equatorial waveguide, ocean dynamics is more important in governing the change of Ts. While T_s is dominated by the Austral annual cycle, the semi-annual period is predominant in the variation of S, as shown in Fig, 5b. The results are consistent with those by Liu and Gautier [1990], using different sets of satellite data covering a different period of time.

The distributions of correlation coefficients between E and T_s are shown in Fig. 4c. For 47 independent pairs of data, a correlation coefficient higher than 0.39 would be significant at a 99% level, Significant positive correlations are found only in the eastern equatorial Pacific and Atlantic near the coasts. These areas are relatively small. Over most of the ocean, there is no significant positive correlation, The negative correlation between E and Ts, found over most of the ocean, is, perhaps, caused by a third factor. This factor could be u, which correlates positively with E (Fig. 4d) but negatively with Ts (Fig. 4f), or q_a which correlates negatively with E (Fig. 4e) but positively with T_s (Fig. 4g). The implication is that, over large areas of the ocean, T_s is not the most direct factor in the seasonal change of evaporation. Atmospheric parameters that have higher variabilities are more important in governing the seasonal changes of E. In the eastern equatorial Pacific and Atlantic, the correlations between E and u are negative and the correlations between E and q_a are weak; the variability of E is dominated by Ts. Over the warm pool in the western Pacific and eastern Indian oceans, the correlations between E and Ts and between E and q_a are both weak; the variation of E is dominated by u. The distribution of correlation coefficients between E and dT_s/dt is shown in Fig. 4h. The distribution is almost identical with the correlation between E and lag T_s (not shown). Over most of the ocean, the correlations are largely negative and relatively strong in mid-latitudes. Evaporation appears to provide important seasonal cooling of the upper ocean. The exception is in the eastern Pacific, just north of the equator where an unexplained zonal band of positive correlation is found.

To elucidate the correlation between E and Ts, their time series at six selected locations are shown with those of u and Aq in Fig. 6. At 40°N, 160°E and 40°S, 40°E, the annual cycles of E are in phase with u and Aq, with lows in summer and broad peaks in winter, in agreement with Eq. 1. They are roughly 90° (three months) off phase with Ts,

which peaks in late summer or autumn. The highs of E are roughly three months ahead of the lows in T_s. Since T_s variation is dominated by the annual cycle (away from the equatorial region) and has a three-month phase difference with dT_s/dt, E has strong negative correlation with the temperature tendency. In the eastern Pacific and Atlantic near the equator, the influence of wind is weak and two examples are shown in Fig. 6. At 10OS, 0°, a phase difference between E and T_s, similar to those at higher latitude, is found, but here the annual cycle of E is completely dominated by Aq and is quite different from the temporal variability of u. At this location, the' annual range of u is relatively small and u does not play an important role in changing E. At 0°, 0°, the seasonal variation of both u and q_a are small and E is in phase with both Aq and Ts; this is the reason for the positive correlation between E and T_s. At 0°, 170°W, shown in Fig. 1 e, the variation is completely dominated by the ENSO signal, The variation of E agrees closely with the variation of Aq with high values during the cold phase of ENSO and low values during the warm phase; negative correlations are the results. Over the warm pool 0°, 150°E, there is no clear annual cycle and the variation of E agrees best with u. The dominant influence of wind on the variation of E was suggested by Liu (1988) and is supported by *in situ* observations (e.g., Meyers et al., 1986; McPaden and Hayes, 1991).

The time series comparisons show that the main factor governing E varies with location; Ts is the dominant factor only over a very limited area and the influence of u and q_a can not be discounted. Over most of the ocean, high T_s does not coincide with high E. The important role played by evaporative cooling in upper ocean heat balance is a probable reason for the negative correlations between E and temperature tendency, Other possible explanations are discussed in Section 8.

7. **ENSO Anomalies**

The correlation coefficients for collocated and contemporary anomalies are shown in Fig, 7. The most striking features are the negative correlations between S and T_s (Fig. 7a) and between E and T_s, (Fig. 7c), in the central equatorial Pacific and with a weak eastward extension north of the equator and a strong extension towards the southeast. These strong local correlations are found in areas of significant flux anomalies during ENSO (see Fig. 4). The negative correlations between the anomalies of S and T_s were observed by Liu and Gautier [1990], Chertock et al. [1991], and others before. They suggest that S anomalies are, perhaps, influenced by local Ts through cloud, as articulated by RC. However, the relation is not universal and does not hold in some surrounding areas with equally warm water or significant Ts anomalies but with no significant S anomalies. The results support the argument that cloud and S anomalies are more directly linked to large-scale circulation than local Ts. The lack of significant positive correlation between S and dT_s/dt (Fig. 7b) suggests an anomalous S has a weak influence in the anomalous change in Ts relative to other factors in Eq. 2, in agreement with Liu and Gautier [1990]. Some positive correlations between S and dT_s/dt are found in the subtropical oceans where Ts anomalies are weak, but they may not be significant.

Positive correlations between anomalies of E and Ts are found only in the eastern equatorial Pacific and Atlantic, as shown in Fig. 7c. In the central equatorial Pacific, the negative correlations between E and Ts again suggest that evaporation is not directly driven by local Ts, even in interannual time scales. Above-normal Ts is found in the same places as lower than normal evaporation and vice versa, in agreement with Liu (1988) based on different sets of data during different ENSO episodes. The variability of other factors, such as u and q_a, must be taken into consideration. There are significant negative correlations between E and the temperature tendency (Fig. 7d), in agreement with Liu and Gautier [1990] albeit weaker than expected. E appears to have a stronger influence on anomalous Ts change than S.

Significant negative correlations are found in the regions where organized deep convection or the ascending branch of the Walker Circulation was displaced during ENSO, but not over the descending branch of large-scale circulation, indicating the importance of large-scale atmospheric circulation. Ascending air has to be compensated by descending air with opposite effect on the fluxes, probably over equally warm water. To examine the role of large-scale circulation, the interannual anomalies of S, E, and Ts averaged over areas encompassing various parts of the Hadley and Walker circulations are compared in Fig. 8 and 9. In Fig. 8a and 9a, the parameters are averaged over the central equatorial Pacific, 5°N to 5°S and 170°E to 130°W, where the ascending branch was displaced during the 1987-1988 ENSO. They clearly show a negative correlation during the ENSO event. The correlation coefficients are -0.76 between the time series in Fig. 8a and -0.63 between the time series in Fig. 9a. The S anomalies during both the warm and cold phases of the 1987-1989 ENSO are largely eliminated as the area of average is expanded (30°N to 30°S, 90°E to 80°W) to include the descending branch of the circulations (Fig. 8b), perhaps because S anomalies in ascending and descending branches cancel each other, as suggested by Fu et al. [1992]. The time series in Fig. 8b have no significant correlation, with a correlation coefficient of -0.02. On the other hand, the E anomalies are preserved, although over a shorter period (Fig. 9b). Although the large negative and positive E anomalies in August 1978 and August 1988 correspond to positive and negative T_s anomalies respectively, the correlation coefficient of -0.14 between the two time series is rather insignificant. The time series in Fig. 8C and 9C are averaged over the same area as Fig. 8b and 9b, but only data with T_s>29°C are used, There are no large S anomalies during the warm and cold phases of ENSO and the correlation coefficient of -0.04 between the S and T_s time series in Fig. 8C is insignificant. Over the warm water, the anomalies of E and T_s are opposite of each other, wtih a correlation coefficient of -0.39. The results illustrate the opposing effect on cloud forcing

within the large-scale circulation; the opposing effects are valid even if we confine the analysis over warm water.

Another way to examine the relation with respect to large-scale circulation is through the distribution of remote correlation coefficient. Ts anomalies averaged in an area between 5°N and 5°S and between170°E and 130°W (shown in Fig, 8a and 9a) were correlated with time series of other parameters at all locations. In the surrounding areas to the east, north, and south of this area, the correlation between the flux and local T_s anomalies are low, but the the remote correlations (not shown) have magnitudes larger than than 0,5, supporting the inference on the importance of large-scale circulation.

The maps of the remote correlation coefficient between the filtered anomalies of T_s (averaged over the area within the black box) and four parameters, S, E, u, and q_a are shown in Figure 10. To make sure that low frequency correlations are not masked by high frequency noise, we attempted to remove the noise by passing the principal components of the anomalies through a low-pass filter and then reconstructing the data field from the filtered components. A 7th order Butterworth Filter (Oppenheim and Schafer, 1975) was used, with a cutoff frequency of 2,25 months, a passband tolerance of 1 db for periods longer than 3 months, and a stopband specification that the signal would be reduced by more than 15 db for periods shorter than 2.19 months. Principal component analysis and filtering were performed for the full length of anomalies available for E, S, Ts, u, q_a, and Aq. The patterns of positive and negative correlations for the non-filtered anomalies (not shown) are the same as those for the filtered anomalies shown in Fig. 10. The net effect of filtering is the accentuation of the correlations, particularly in areas outside the equatorial Pacific where the ENSO signal is not so prominent. While filtering distorted the relative magnitude of the variance, it helped to reveal the low frequency variations and to interpret the temporal correlations and their

distributions. The filtered data are used only to illustrate the relative positions of the positive and negative anomalies.

Similar patterns are found in all the correlations shown in Fig. 10. The correlations in the central equatorial Pacific, with strong extension to the southeast and a weaker extension eastward just north of the equator and with an area of weak or opposite correlation embedded in the east, are surrounded on three sides by areas of opposite correlations. The pattern is associated with dipole oscillation of large-scale convection and circulation as observed by other investigators, particularly in the anomalies of outgoing longwave radiation [e.g., Lau and Chan, 1983], with eastward migration of deep convection from the western Pacific, southeast extension of the SPCZ and the equatorward movement of the ITCZ during the warm phase of ENSO and the reverse during the cold phase, The eastern equatorial Pacific is occupied by dry air; deep convection rarely occurs.

To illustrate the temporal correlations, filtered time series of S and T_s are compared at eight selected locations in Fig. 11. At the central equatorial Pacific (Fig 11a) and SPCZ extension (Fig, 11 b), organized convections were displaced during ENSO. At these locations, a warm phase in 1987 corresponds to lower radiative heating and a cold phase in 1988 corresponds to higher radiative heating. Large anomalies in S and strong negative correlation between anomalous S and T_s are found before filtering. Embedded in the region of high negative correlation is a region of low correlation typified by the time series at 5°S and 100°W, shown in Fig. 11c. In this area, the Ts anomaly has similar temporal variation as the immediate surrounding area, but the ENSO signal in S is ill defined. At locations further out (Fig. 11 d, f, g, h), the phases of T_s anomalies are opposite to that in the central equatorial Pacific, cold during 1987 and warm during 1988. Over the western Pacific, at 5°S and 155°E (Fig. 1 id), the phase of Ts anomalies is

opposite to those in the central Pacific but the phase of S anomalies is the same. The positive local correlation and negative remote correlations reflect the extension of S anomalies eastward of Ts anomalies in the central equatorial Pacific as discussed in Section 5. Further to the west, at the equator and 130°E (Fig. 11 f), the local correlations are negative but the remote correlations are positive. Although Ts anomalies here remain opposite in phase to those in the central equatorial Pacific, the phase of S has changed. The variations at 20°N and 160°E and at 20°S and 160°E (Fig, 11 g and h) are similar to Fig. 11f. Further west, in the Arabian Sea, at the equator and 90°E (Fig. 1 le), the variations are similar to those in the central equatorial Pacific, with a warm phase in 1987 and a cold phase in 1988 but no clear ENSO signal in S.

The filtered anomaly time series of E, Ts, u, and q_a at six locations, for the four-year period, are compared in Fig. 12. At the equator and 170°W (Fig. 12a), typical of the central Pacific, Ts shows a warm phase in 1987 followed by a cold phase in 1988, opposite in phase to E, u, and q_a. At this location, Aq has the best correlation with E and is likely to be the most influential factor on the anomalous change of E. The variations of SPCZ extension at 20°S and 120°W (Fig. 12 b) are very similar to those shown in Fig. 12a. In the eastern equatorial Pacific, typified by the time series at 5°S and 100”W (Fig. 12c), u and q_a anomalies are small and E anomalies follow the variation of T_s. Surrounding the region of negative remote correlation is the region of positive remote correlation represented by the time series at the three locations in the right column of Fig. 12. In the western Pacific at the equator and 130°E (Fig. 12b), E correlates best with u and, therefore, is largely driven by u. In the north at 20”N and 160°E and in the south at 20°S and 160°E, the variations of E follow most closely those of Aq. Similar to the seasonal variations discussed in Section 7, the anomalies of E are likely to be driven by different factors in different regions affected by large-scale circulations.

8. Discussion and Conclusion

The correlations between the two major surface heat flux components and T_s do not support simple one-dimensional local feedback postulations; the postulations require (1) that T_s is the dominant drive of flux changes and (2) that the fluxes are the most important factors governing Ts changes. The differences in geographical distribution between S and Ts and the lack of negative temporal correlation between them imply that Ts in not the dominant factor in the seasonal variation of local cloud and S; S is mainly changed by the solar incident angle. However, solar heating is a main factor in the seasonal variation of local Ts, except in a zonal belt approximately 5° from the equator where ocean dynamics may play a more important role. For ENSO, S anomalies are not always co-located with T_s anomalies and negative correlations are present in some but not all of the warm water areas. The lack of positive correlation between anomalies of S and temperature tendency implies that "the local effect of anomalous solar heating may not be significant compared with changes in ocean dynamics and other flux components during ENSO. The ubiquitous negative correlations between E and T_s and between E and dT_s/dt, in both monthly means and anomalies, suggest that T_s is not the dominant factor in changing E but imply possible significant influence of evaporation on upper ocean heat balance and local change of Ts. The results are in agreement with Liu and Gautier (1990) who used data from a different time period and derived from different spaceborne sensors.

The results also demonstrate that simple correlation between the flux and Ts may not be sufficient to reveal causality. The negative correlation between E and Ts may be the result of other factors. E is found to be positively correlated with u and negatively correlated with q_a over most of the ocean. Negative correlation between Ts and u and positive correlation between Ts and q_a result in negative correlation between Ts and E.

Over the tropical oceans, ascending air and deep convection overlie warm water and draw surface convergence, which lowers u and raises q_a, or the surface temperature gradient sets up pressure differentials and convergence that facilitate convection (Lindzen and Nigam, 1987); the low E over high T_s is an indirect consequence. The negative correlation may also be the indirect result of ocean dynamics. Stronger wind forcing may change thermocline depth and entrainment intensity, and thus upper ocean heat balance.

Although RC found increase in cloud forcing at the same location as increase in T_s during ENSO (and their finding is supported by the negative correlations between anomalous Ts and S we found in the central Pacific), any explanation based on local feedback may not be correct because the increase in cloud forcing is caused by large-scale circulation rather than local T_s. The remote correlations shown in Fig, 11 suggest that cloud increase is caused by the shifting of organized convection in the ascending branches of Walker and Hadley Circulations which largely overlie warm water. There are areas of equally warm water in the eastern tropical Pacific, but there are no significant S anomalies because atmospheric subsidence prevents high cloud formation. Due to conservation of mass, the rising air in convection must be compensated by subsiding air. When averaged over both the ascending and descending branches of the large-scale circulation, the anomalies of S were found to almost cancel out, despite net changes in T_s anomalies.

High T_s does not necessarily correspond to high E or vice versa; this is true in geographical distribution, in the seasonal changes, and in the ENSO anomalies. The assumptions of constant u and r (Eq. 1) in the conceptual models of ocean thermostat are spurious. The significance of wind variability over the warm ocean is well documented, both in observation (e.g., Meyers et al. 1986) and in model simulation (e.g., Seager, 1989). The impact of r variability on computation of E was studied by Liu and Niiler

[1990]. A small error in r or a small percentage error in q_a corresponds to a large percentage error in Δq because q_a is large compared with Δq over warm oceans and E depends linearly on Δq and not q_a. In the tropical oceans, it was found that a ± 5 % error in r causes errors in E that are comparable with the annual and interannual signals. In high latitude ocean, Liu and Niiler [1990] also found that the annual cycle of q_a is out of phase with q_s; E (or Δq), therefore, leads T_s.

The recent debate on ocean thermostat addresses global warming, and the analysis were entirely confined to low-frequency variabilities from seasonal to decadal. However, large high-frequency fluctuations have been observed in convection over the warm pool of western Pacific [e.g., Young et al., 1992]. Using monthly-mean parameters in estimating latent heat flux with the bulk formula and in computing the correlation coefficient neglect these high-frequency variances and may introduce erroneous results. However, there has been no clear evidence as to significant long-term and large-scale effects of these short-lived small-scale variances, If the newly installed humidity and radiation sensors in TOGA Tropical Atmosphere Ocean (TAO) Array [McPhaden, 1993] could provide sufficient accuracy and stability in the long term, temporal multiscale interaction could be examined in the future. The TOGA-COARE (Tropical Ocean Global Atmosphere - Coupled Ocean and Response Experiment) will also provide the observations to understand spatial variation and multiscale processes in the warm pool. It is difficult to separate cause and effect and to isolate the feedback mechanism with available data, as pointed by Stephens and Slingo [1992]. This study is only one step to further our understanding of the processes that maintain the warmest sea surface temperature using a unique set of data,

The relation between surface fluxes and Ts is not universal, Neither E nor S alone appear to be sufficient to keep the ocean at an equilibrium temperature. The

collocated changes of cloud forcing and T_s observed by RC are likely to be the result of atmospheric circulation (shifting of tropical convective systems) and ocean dynamics (propagation of equatorial waves) during ENSO.

Acknowledgment

This study was performed at the Jet Propulsion Laboratory, California Institute of Technology, under contract with the National Aeronautics and Space Administration (NASA). It was supported by the Interdiscipline Science Investigation of the Earth Observing System and Global Change Data Analysis Program of NASA. The surface solar flux was computed at the Goddard Institute of Space Studies. We are grateful to William Rossow and Rong Fu for their comments and suggestions.

Reference

Betts, A. K., and W. Ridgway, Climatic equilibrium of the atmospheric convective boundary layer over a tropical ocean, J. *Atmos. Sci.,* **46,2621-2641, 1989.**

Bishop, J. K. B., and W. B. Rossow, Spatial and temporal variability of global surface solar irradiance. *J. Geophys. Res.,* 96, 16839-16858, 1991.

Bradley, E.F., P.A. Coppin, and J.S. Godfrey, Measurement of sensible and latent heat flux in the western equatorial Pacific Ocean, *J. Geophys. Res.,* **96,3375-3389, 1991.**

Cayan, D, R., Latent and sensible heat flux anomalies over the Northern Oceans; driving the sea surface temperature, *J. Phys. Oceanogr., 22, 859-881,* 1992,

Chertock, B:, R. Frouin, and R. C. J. Somerville, Global monitoring of net solar irradiance at the ocean surface: climatological variability and the 1982-1983 El Niño, *J. of Climate, 4,639-650., 1991.*

Cornejo-Garrido, A.G., and P.H. Stone, On the heat balance of the Walker Circulation, *J. Atmos. Sci.,* 34, 1155-1162, 1977.

Esbensen, S.K.,and R.W. Reynolds, 1981: Estimating monthly average air-sea transfer of heat and momentum using the bulk aerodynamic method, *J. Phys. Oceanogr., 11,457-465, 1981.*

Fleagle, R. G., and J.A. Businger, *An Introduction to Atmospheric Physics,* Academic Press, New York, 62-63, 1963.

Friehe, C. A., and K.F. Schmitt, Parameterization of air-sea interface fluxes of sensible heat and moisture by bulk aerodynamic formulas, *J. Phys. Oceanogr., 12, 801-809, 1976,*

Fu, R., A.D. Del Genio,W.B. Rossow, and W.T. Liu, Cirrus-cloud thermostat for tropical sea surface temperatures tested using satellite data, *Nature, 358, 394-397, 1992.*

Gadgil, S., P.V. Joseph, and N.V. Joshi, Ocean-atmosphere coupling over monsoon regions, *Nature, 312, 141-143, 1984.*

Graham, N. E., and T.P. Barnett, Sea surface temperature, surface wind divergence, and convection over tropical oceans, *Science, 2.?8, 657-659, 1987.*

Godfrey, J.S. and E.J. Lindstrom, The heat budget of the equatorial western Pacific surface mixed layer, *J. Geophys. Res., 94, 8007-8017,* 1989.

Hsiung, J., mean surface energy fluxes over the global ocean, *J. Geophys. Res., 91, 10585-10606, 1986.*

Hsu, S. A., and B.W. Blanchard, The relationship between total precipitable water and surface-level humidity over the sea surface; A further evaluation, *J. Geophys. Res., 94, 12539-14545, 1989.*

Katsaros, K. B., and J, DeCosmos, Water vapor flux from the sea at high wind speeds, *Proc. ICSU/WMO International Symp. on Tropical Cyclone Disasters,* J. Lighthill and Z. Zheng (eds.), in press, 1993.

Lau, K, M., and P.H. Chan, Short-term climate variability and atmospheric teleconnections from satellite-observed outgoing longwave radiation. Part I: simultaneous relationships, *J. Atmos. Sci., 40, 2735-2750, 1983.*

Leetma, A., The role of local heating in producing temperature variation in the offshore waters of the eastern tropical Pacific, *J. Phys. Oceanogr., 13,467-473,* 1983,

Lindzen, R. S., and S. Niagam, On the role of sea surface temperature gradients in forcing low-level winds and convergence in the tropics, *J. Atmos. Sci, 44,2418-2436, 1987.*

Liu, W. T., Statistical relation between monthly precipitable water and surface-level humidity over global oceans, *Mon. Wea. Rev.,* 114, 1591-1602, 1986.

Liu, W. T., Moisture and latent heat flux variabilities in the tropical Pacific derived from satellite data, *J. Geophys. Res., 93, 6749-6760.1988.*

Liu, W. T., Remote sensing of turbulence flux, *Surface Waves and Fluxes,* Vol. H, G.L. Geenaert and W.J. Plant (eds.), Kluwer Academic Press, 293-309, 1990.

Liu, W. T., and C. Gautier, Thermal forcing on the tropical Pacific from satellite data, *J Geophys. Res., 95, 13209-13217* and 13569-13580, 1990.

Liu, W, T., K.B. Katsaros, and J.A. Businger, Bulk Parameterization of air-sea exchanges of heat and water vapor including the molecular constraints at the interface, *J. Atmos. Sci., 36, 1722-1735, 1979.*

Liu, W.T. and P.P. Niller, The sensitivity of latent heat flux to the air humidity approximations used in ocean circulation models, *J. Geophys. Res.*, 95, 9745-9753, 1990.

Liu, W.T., W. Tang, and P.P. Niiler, Humidity profiles over ocean, *J. Climate, 4, 1023-1034, 1991.*

Liu, W,T., W. Tang, and F.J. Wentz, Precipitable water and surface humidity over global oceans from SSMI and ECMWF, *J. Geophys. Res., 97,* 2251-2264, 1992.

McClain, E. P., W.G. Pichel, and C.C. Walton, Comparative performance of AVHRR-based multichannel sea surface temperatures. *J. Geophys. Res.*, 90, 11587-11601, 1985.

McPhaden, M. and S.P. Hayes, On the variability of winds, sea surface temperature, and surface layer heat content in the western equatorial Pacific, *J. Geophy. Res.*, 96, 3331-3342, 1991.

McPhaden, M. 1993: TOGA-TAO and the 1991-93 El Nino - Southern Oscillation event. *Oceanography, 6,36-43, 1993.*

Meyers, G., J.R. Donguy, and R. K. Reed, Evaporative cooling of the western equatorial Pacific ocean by anomalous winds, *Nature, 323,523-526, 1986.*

Newell, R,E., Climate and the ocean, *Amer. Sci., 67,405-416, 1979.*

Niiler, P., and J. Stevenson, The heat budget of tropical ocean warm-water pools, *J. Mar. Res.*, 40, *sup.*, 465-480; 1982.

Press, W. H., B.P. Flannery, A, Teukolsky, and W. T. Vetterling, *Numerical Recipes,* Cambridge Univ. Press, 45, 1989.

Priestley, C. H. B., The limitation of temperature by evaporation in hot climates, *Agric. Meteor.* 3,241-246, 1966.

Oppenheim, A, V., and R. W. Schafer, *Digital Signal Processing,* Prentice-Hall, Inc., Englewood Cliffs, New Jersey,211 -218, 1975.

Ramanathan, V., and W, Collins, Thermodynamic regulation of ocean warming by cirrus clouds deduced from observations of the 1987 El Niño, *Nature, 351, 17-32, 1991.*

Ramanathan, V., and W. Collins, Thermostat and global' warming, *Nature, 357, 649, 1993,*

Reynolds, R. W., A real-time global sea surface temperature analysis. *J. Clim., 1,75-86,* 1988.

Rossow, W. B., and R.A. Schiffer, ISCCP cloud data products, *Bull. Am. Meteor. Sot., 72,* 2-20, 1991.

Seager, R., Modeling tropical Pacific sea surface temperature: 1970-87, *J. Phys. Oceanogr., 19,419-434,1989.*

Stephens, G., and T, Slingo, An air-conditioned greenhouse, *Nature, 358,369-370, 1992.*

Trenbeth, K. E., 1992, Prepared statement, *Global Change Research: the Role of Clouds in Climate Change,* Hearing before the Committee on Commerce, Science, and transportation, United States Senate, S. HRG. 102-564, U.S. Government Printing Office, Washington, 22-33, 1992

Wallace, J. M., Effect of deep convection on the regulation of tropical sea surface temperature, *Nature, 357,230-231, 1992.*

Waliser, D. E., and N. E. Graham, Convective cloud systems and warm-pool SSTS: coupled interactions and self-regulation, *J. Geophys. Res.,* in press, 1993.

Waliser, D. E., N.E. Graham and C. Gautier: Comparison of the highly reflective cloud and outgoing longwave data sets for use in estimating tropical deep convection, *J. Climate, 6,331-353, 1993.*

Weare, B. C., Interannual variation in net heating at the surface of the tropical Pacific Ocean, *J. Phys. Oceanogr., 13,873-885, 1983.*

Weare, B. C., P.T. Strub, and M.D. Samuel, *Marine Climate Adas of the Tropical Pacific Ocean,* Contribution to Atmospheric Sci. No. 20, Univ. of California at Davis, 147 pp, 1981.

Young, G. S., D.V. Ledvina, and C.W. Fairall, Influence of precipitating convection on the surface energy budget observed during a tropical ocean global atmosphere pilot cruise in the tropical western Pacific ocean, *J. Geophys. Res., 97,9595-9603,* 1992.

Figure Captions

Fig. 1 Bin-averaged net solar flux (upper) and latent heat flux (lower) as functions of sea surface temperature, for 0.5°C sea surface temperature bins, with standard deviations (error bars) and population of the bins also shown,

Fig. 2 Monthly means of net solar flux (upper), sea surface temperature (center) and latent heat flux (lower) for July 1989 (left) and January 1990 (right), typical of boreal summer and winter.

Fig. 3 Anomalies of net solar flux (upper), sea surface temperature (center), and latent heat flux (lower) for July 1987 (left) and September 1988 (right), during the warm and cold phases of an El Niño Southern Oscillation episode.

Fig. 4 Correlation coefficients between various monthly-mean parameters.

Fig. 5 Time series comparison of monthly-mean net solar flux and sea surface temperature at selected locations.

Fig. *6* Time series comparison of monthly-mean latent heat flux (black), sea surface temperature (red), wind speed (green), and sea-air humidity difference (blue), at selected locations.

Fig. 7 Correlation coefficients between anomalies of solar flux and sea surface temperature (upper left); solar flux and temperature tendency (upper right); latent heat flux and sea surface temperature (lower left); latent heat flux and temperature tendency (lower right).

Fig. *8* Time series comparison of sea surface temperature and net solar flux anomalies, averaged over various geographical areas and conditions.

Fig. *9* Same as Fig. 8 but for latent heat flux instead of net solar flux.

Fig. 10 Correlation coefficients between anomalies of sea surface temperature averaged over the area indicated by the black rectangle (5°N to 5°S, 170°E to 130°W) and anomalies of net solar flux (upper left); latent heat flux (upper right); wind speed (lower left), air humidity (lower right). High-frequency variations of the anomalies were filtered out.

Fig. 11 Time series comparison of filtered anomalies of net solar flux and sea surface temperature at selected locations.

Fig. 12 Time series comparison of filtered anomalies of latent heat flux (black), sea surface temperature (red), wind speed (green), and sea-air humidity difference (blue) at selected locations,

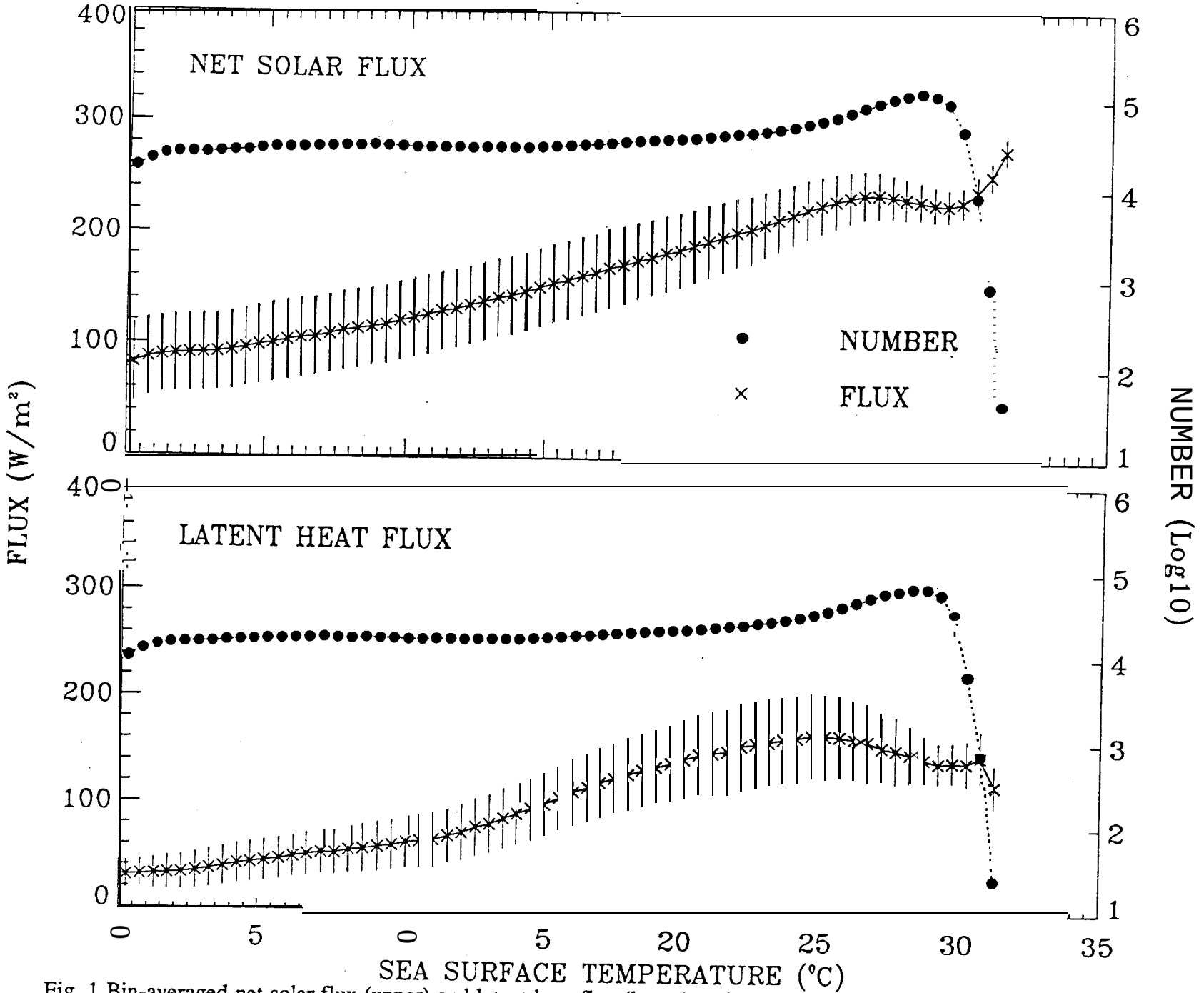

Fig. 1 Bin-averaged net solar flux (upper) and latent heat flux (lower) as functions of sea surface temperature, for 0.5°C sea surface temperature bins, with standard deviations (error bars) and population of the bins also shown.

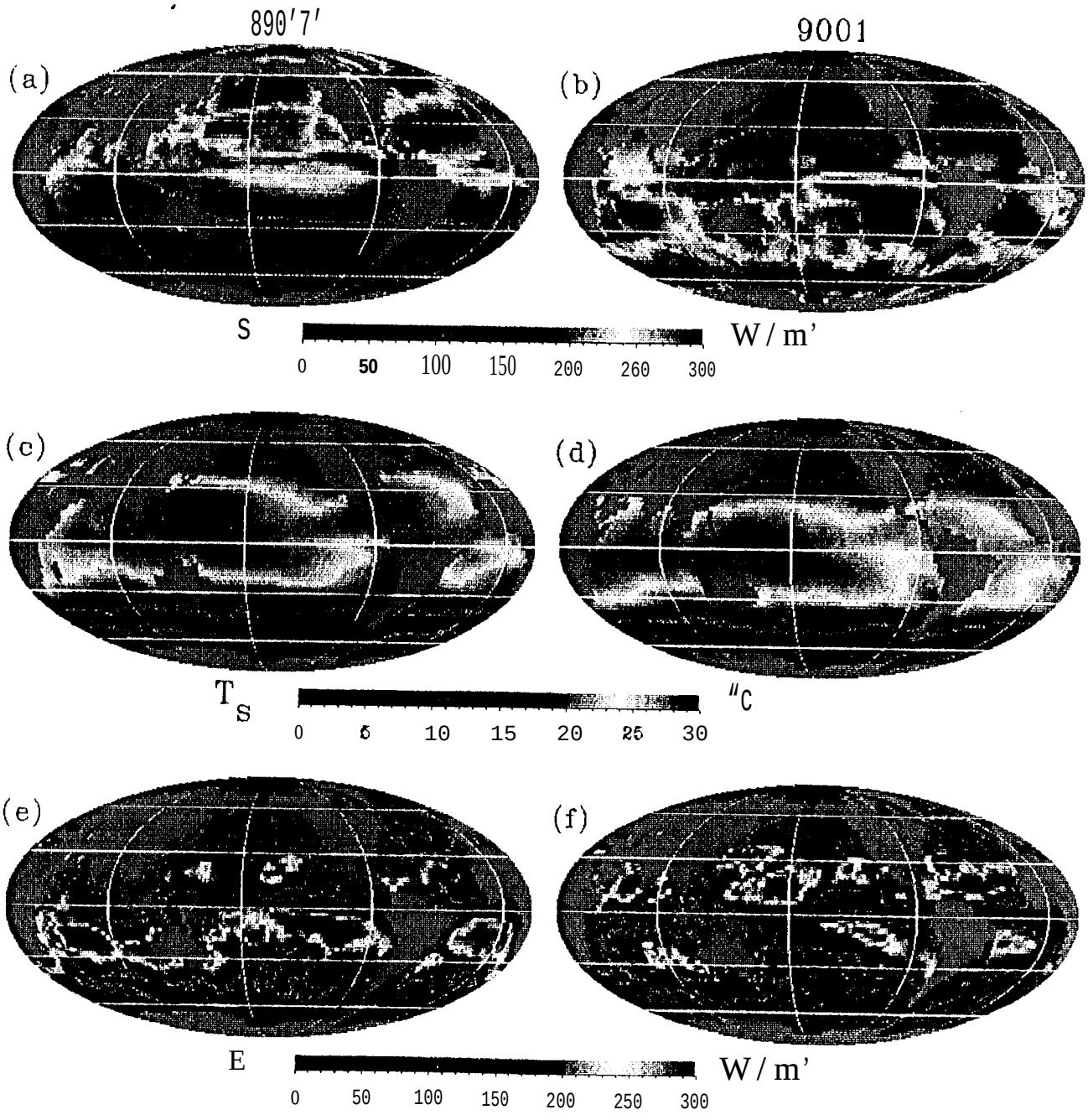

Fig. 2 Monthly means of net solar flux (upper), sea surface temperature (center) and latent heat flux (lower) for July 1989 (left) and January 1990 (right), typical of boreal summer and winter.

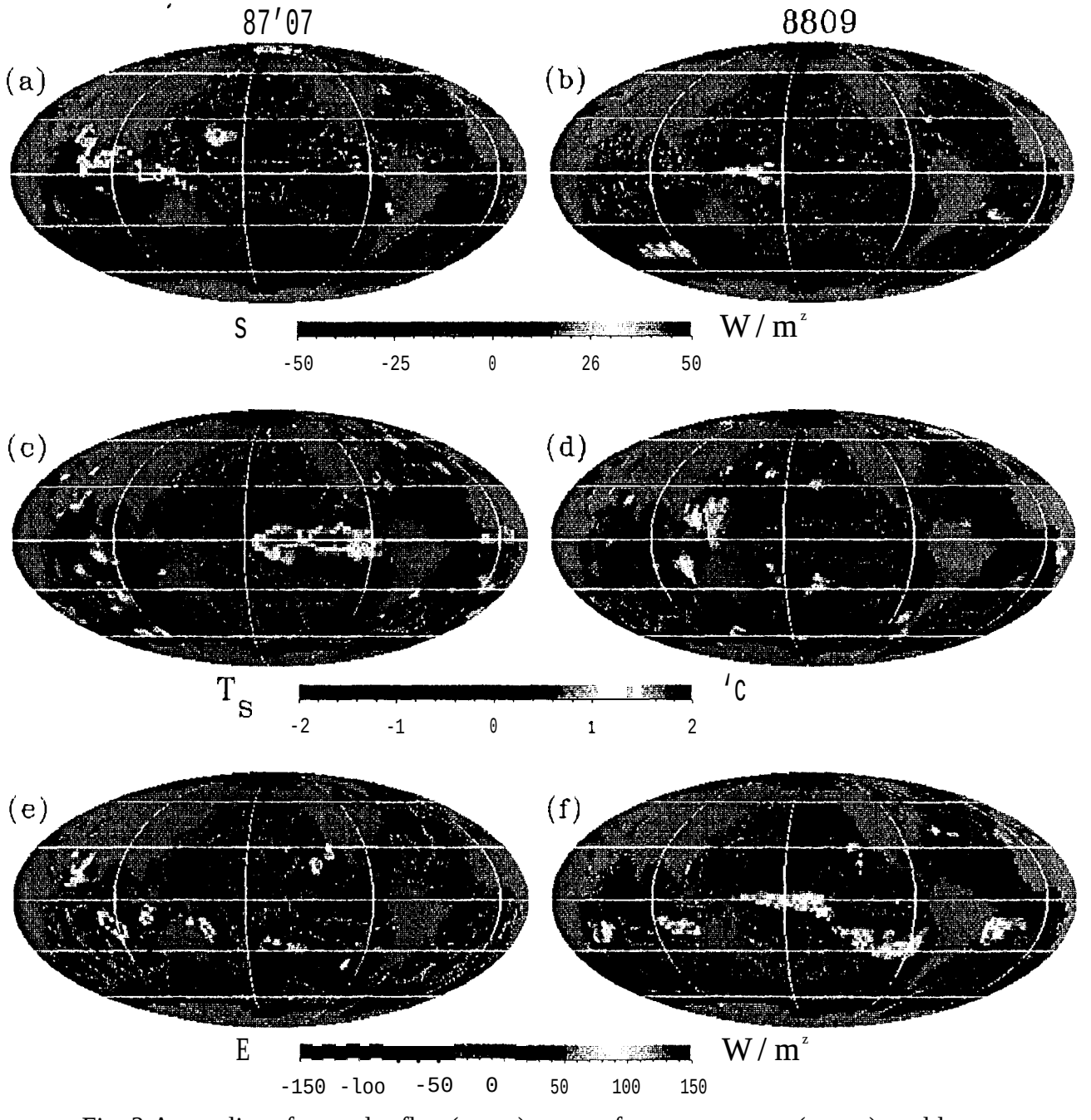

Fig. 3 Anomalies of net solar flux (upper), sea surface temperature (center), and latent heat flux (lower) for July 1987 (left) and September 1988 (right), during the warm and cold phases of an El Niño Southern Oscillation episode.

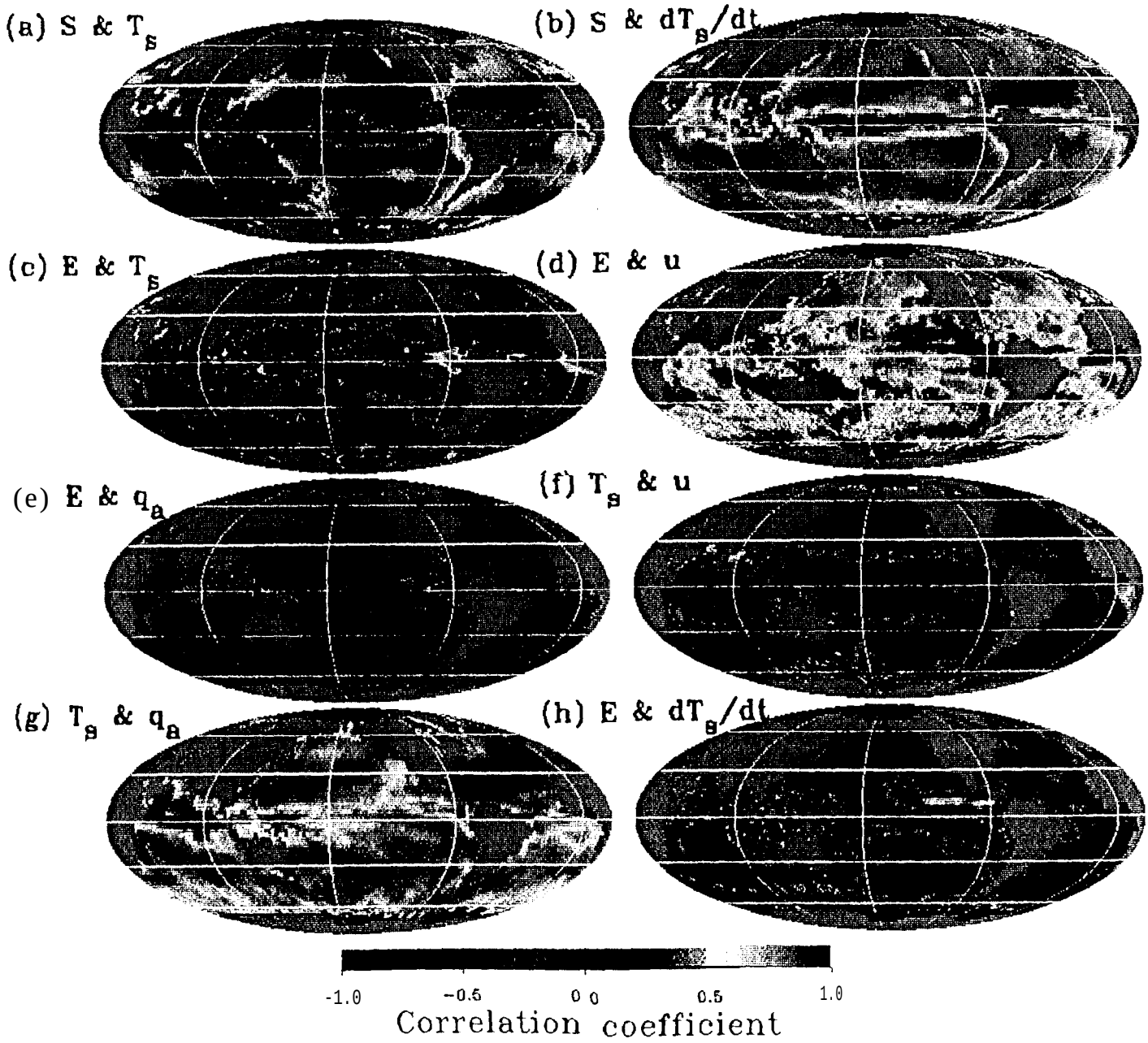

Fig. **4** Correlation coefficients between various monthly-mean parameters.

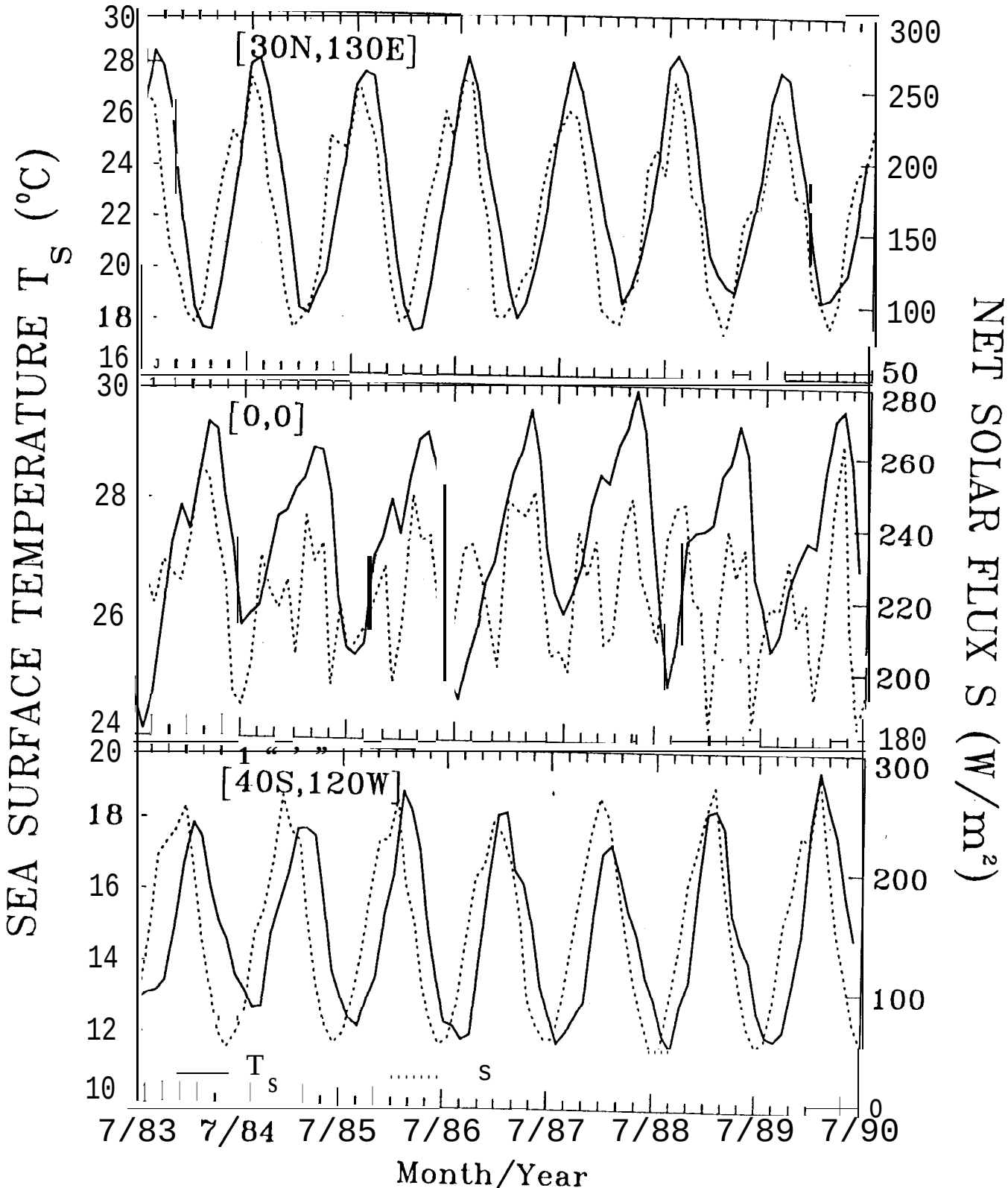

Fig. 5 Time series comparison of monthly-mean net solar flux and sea surface temperature at selected locations.

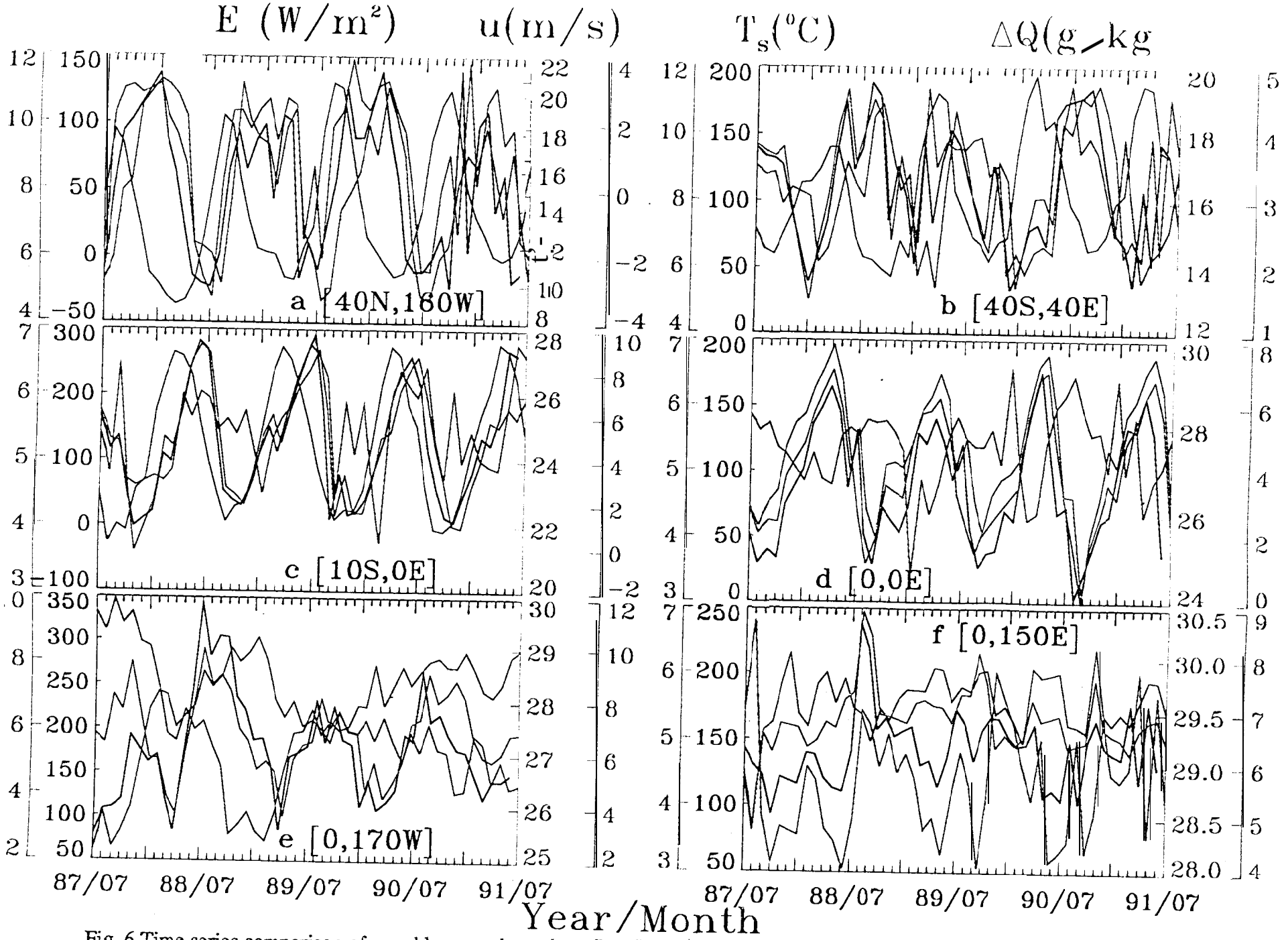

Fig. 6 Time series comparison of monthly-mean latent heat flux (black), sea surface temperature (red), wind speed (green), and sea-air humidity difference (blue), at selected locations.

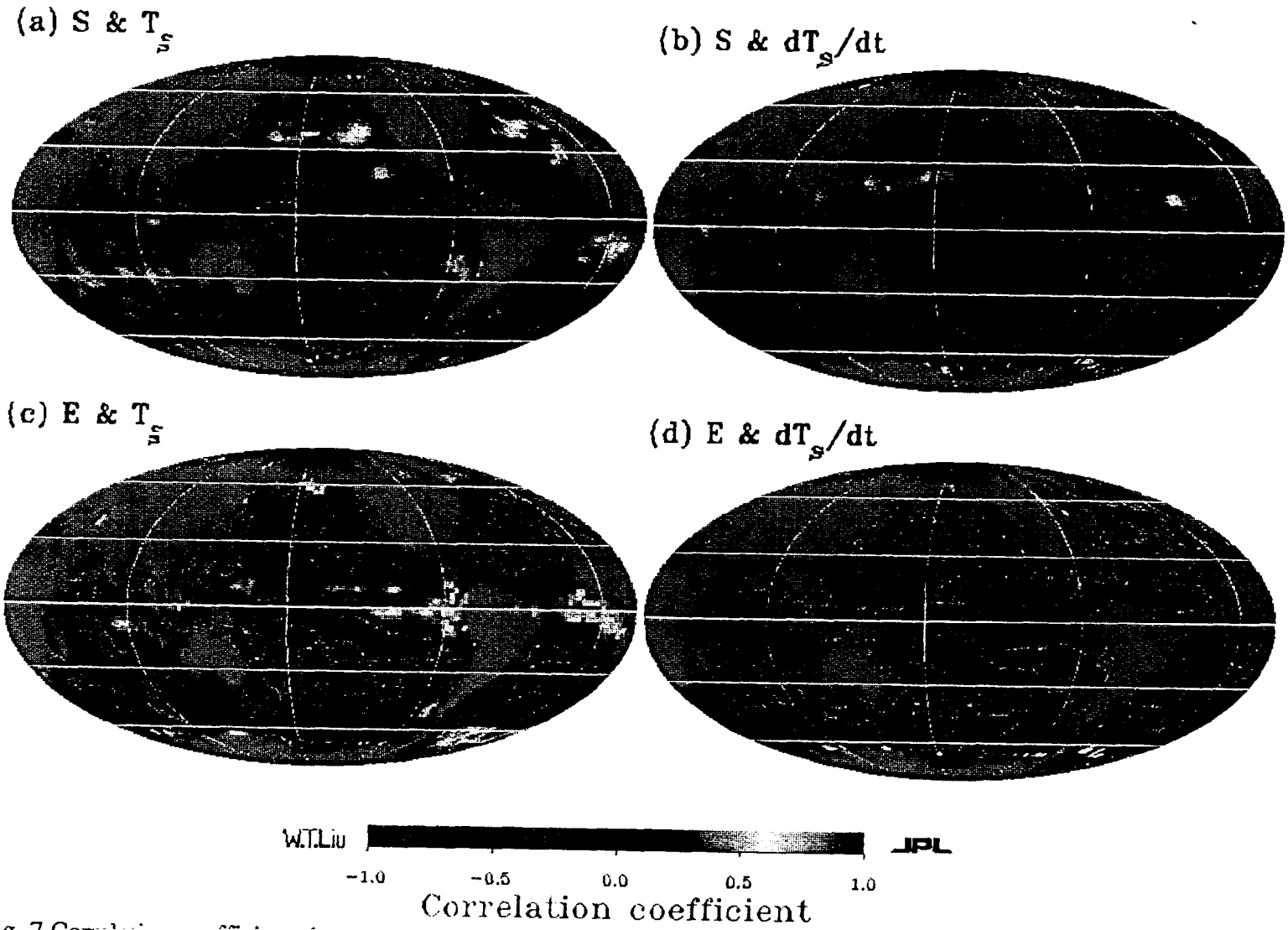

Fig. 7 Correlation coefficients between anomalies of net solar flux and sea surface temperature (upper left); net solar flux and temperature tendency (upper right); latent heat flux and sea surface temperature (lower left); latent heat flux and temperature tendency (lower right).

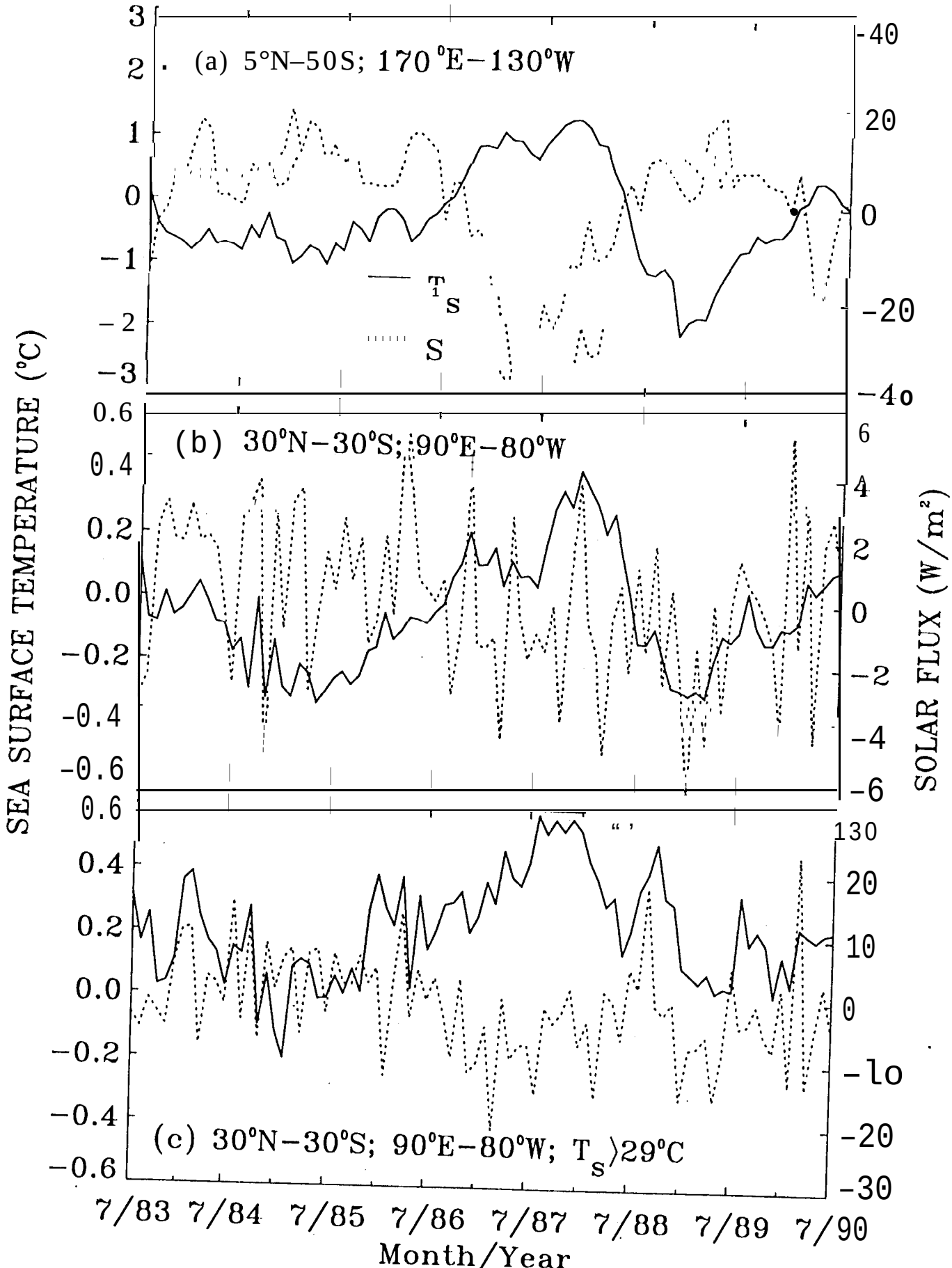

Fig. 8 Time series comparison of sea surface temperature and net solar flux anomalies, averaged over various geographical areas and conditions.

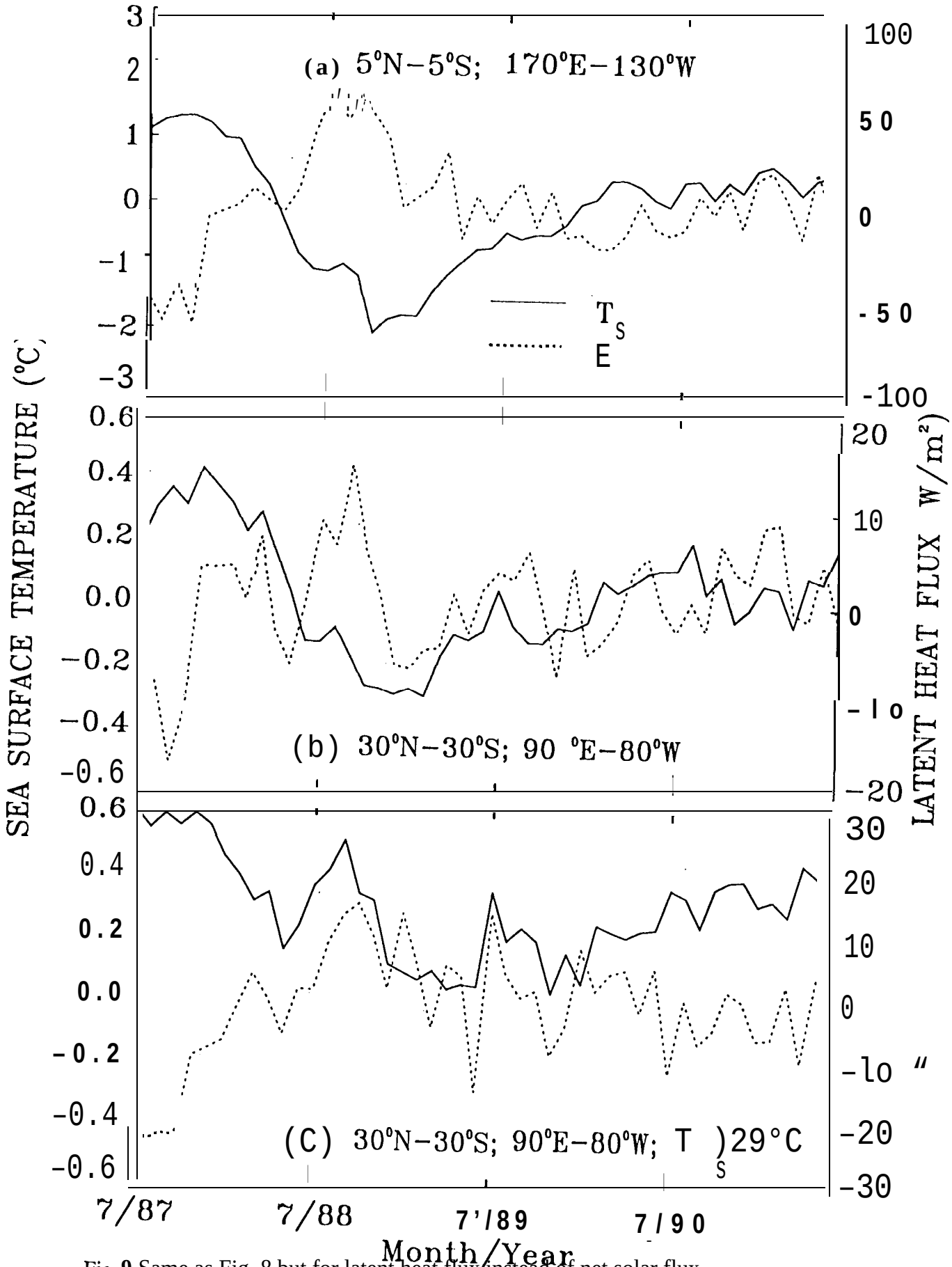

Fig. 9 Same as Fig. 8 but for latent heat flux instead of net solar flux.

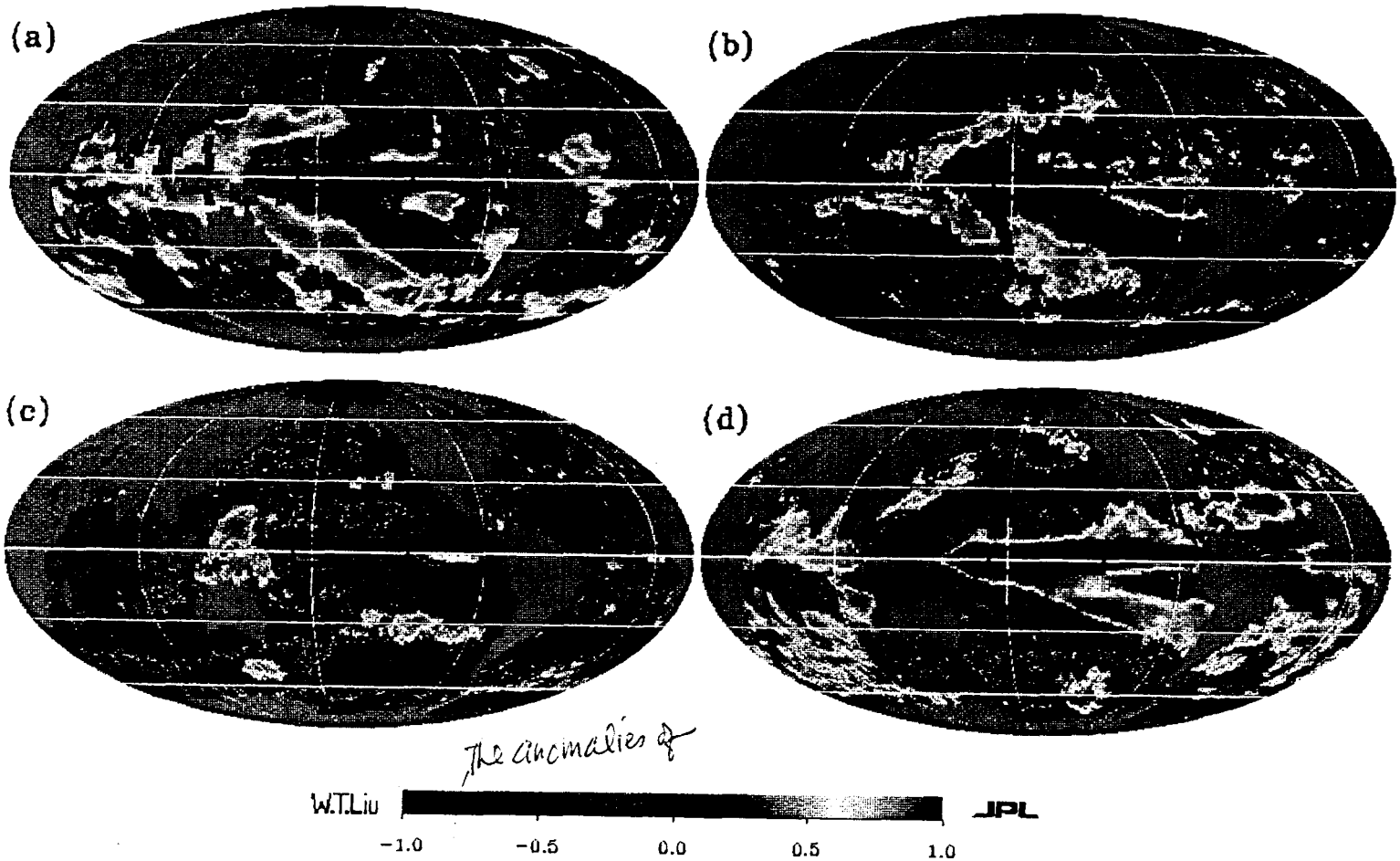

Fig. 10 Correlation coefficients between sea surface temperature averaged over the area indicated by the black rectangle (5°N to 5°S, 170°E to 130°W) and net solar flux (upper left); latent heat flux (upper right); wind speed (lower left), air humidity (lower right). High-frequency variations of the anomalies were filtered out.

the anomalies of

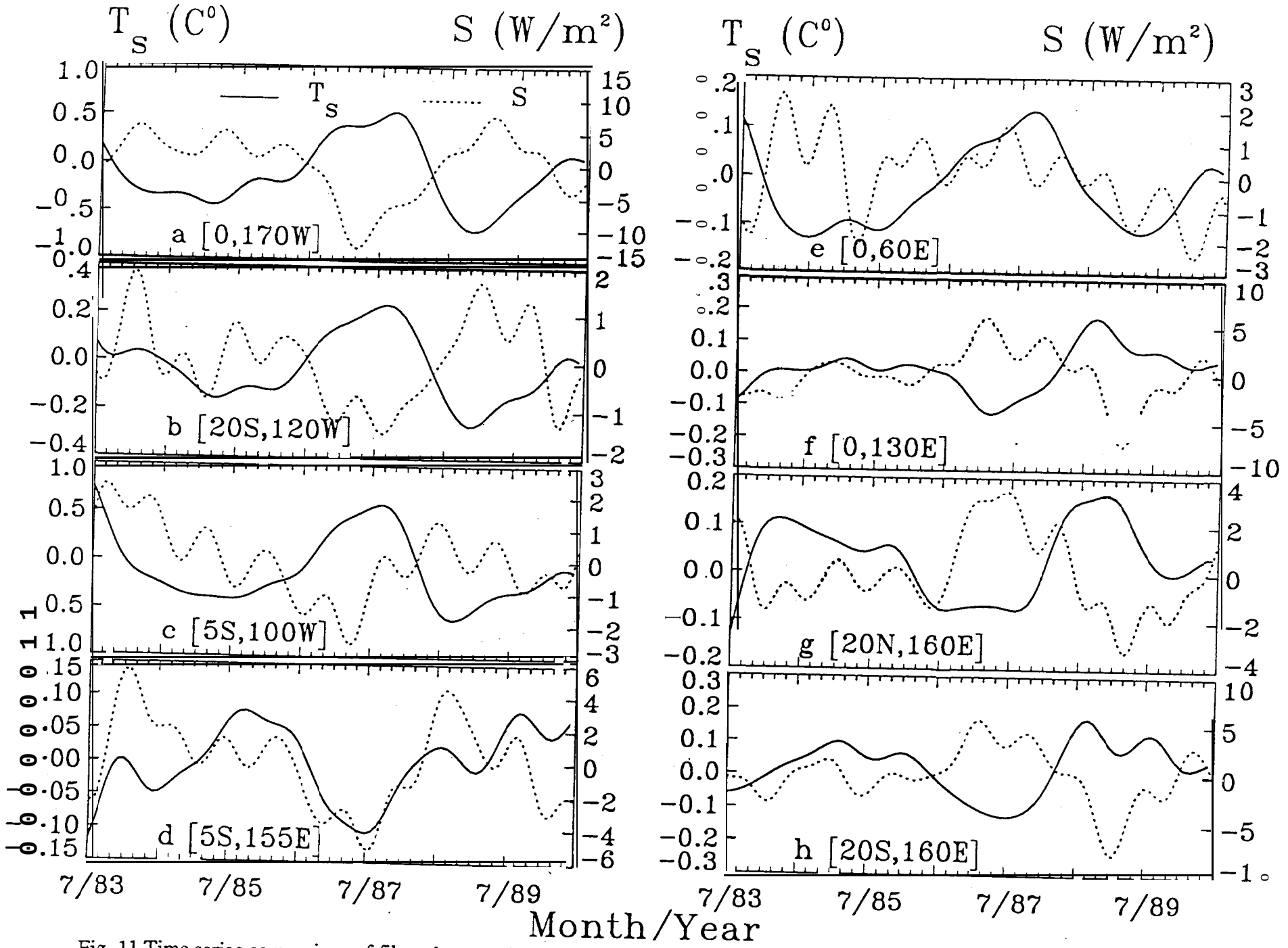

Fig. 11 Time series comparison of filtered anomalies of solar flux and sea surface temperature at selected locations.

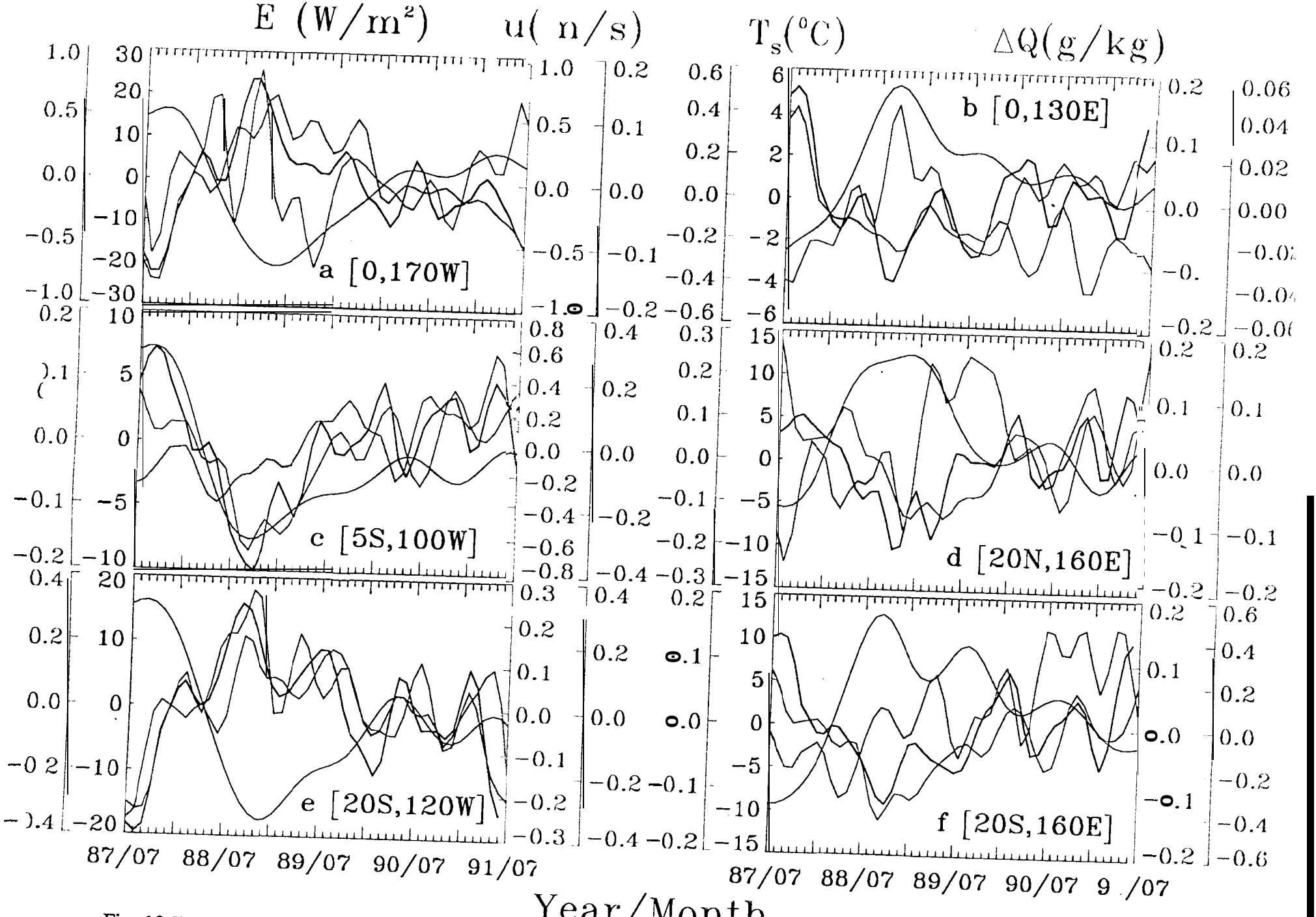

Fig. 12 Time series comparison of filtered anomalies of latent heat flux (black), sea surface temperature (red), wind (green), and sea-air humidity difference (blue) at selected locations.